

Automated Stability Analysis of Piecewise Affine Dynamics Using Vertices

Pouya Samanipour and Hasan A. Poonawala

Abstract—This paper presents an automated algorithm to analyze the stability of piecewise affine (PWA) dynamical systems due to their broad applications. We parametrize the Lyapunov function as a PWA function, with polytopic regions defined by the PWA dynamics. Using this parametrization, stability conditions can be expressed as linear constraints restricted to polytopes so that the search for a Lyapunov function involves solving a linear program. However, a valid Lyapunov function might not be found given these polytopic regions. A natural response is to increase the size of the parametrization of the Lyapunov function by dividing regions and solving the new linear program. This paper proposes two new methods to divide each polytope into smaller ones. The first approach divides a polytope based on the sign of the derivative of the candidate Lyapunov function, while the second divides it based on the change in the vector field of the PWA dynamical system. In addition, we propose using Delaunay triangulation to achieve automated division of regions and preserve the continuity of the PWA Lyapunov function. Examples involving learned models and explicit MPC controllers demonstrate that the proposed method of dividing regions leads to valid Lyapunov functions with fewer regions than existing methods, reducing the computational time taken for stability analysis.

I. INTRODUCTION

Piecewise affine (PWA) dynamical systems have gained popularity in robotics [1] and the automotive industry [2] due to their wide applications. PWA concepts are utilized in advanced controllers, including gain-scheduled flight control systems [3] and Takagi-Sugeno fuzzy systems [4]. Affine systems with control saturation can be expressed using PWA dynamics, enabling effective synthesis of controllers through explicit model predictive control (MPC) [5]. However, obtaining a Lyapunov function for stability guarantees with explicit MPC can be challenging. Alternatively, there is an increasing trend in using supervised machine learning methods for learning dynamics and controllers [6], [7]. Neural networks (NN) with the rectified linear unit (ReLU) activation functions have been employed to convert closed-loop dynamics into PWA dynamics [8]. The stability of these methods, however, is not guaranteed, emphasizing the need to develop an automated approach to finding Lyapunov functions for learned models, including ReLU networks and explicit MPC.

Sampling-based methods [9]–[11] are prevalent for learning Lyapunov functions. The Lyapunov function is learned from finite samples, and this function must meet the stability

conditions at all states, therefore verification is a critical component of the analysis. Verification can be performed in an inexact manner using relaxed convex problems [12] or in an exact manner using Satisfiability Modulo theories (SMT) and Mixed-Integer Programs (MIP) [9], [13]–[15]. The exact verifier certifies the Lyapunov function or generates counterexamples violating the stability conditions. Counterexamples can be incorporated into training samples for iterative learning. However, the computational complexity of the verifier remains a challenge.

An alternative to the learning approach is to parameterize the Lyapunov function and solve it as an optimization problem [16]–[18]. The Sum of Squares (SOS) method is employed to find the Lyapunov function for nonlinear dynamics [16], but it can be computationally complex. A piecewise quadratic (PWQ) parameterization of the candidate Lyapunov function is proposed in [17], [18]. However, these methods must deal with the conservatism of the S-procedure, and the results are limited to two-dimensional examples.

Instead of relying on the PWQ Lyapunov function, [19] utilized the PWA function to parameterize the Lyapunov function. An algorithm has been developed for finding a PWA Lyapunov function using partition refinement in [20]. A method for calculating the Lyapunov function for conewise PWA dynamics was proposed by [21]. The dynamics and controller of PWA have been parameterized as a ReLU in [8]. The Lyapunov function and the controller are found by parameterizing Lyapunov conditions as quantifier-free constraints for a bilinear quadratic optimization problem [8]. Although the Lyapunov condition for the PWA Lyapunov function can be expressed without conservatism, the PWQ Lyapunov function receives more attention in the literature.

The refinement process in the context of Lyapunov stability analysis presents several challenges, such as preserving the continuity of the candidate Lyapunov function and dividing complex polytopes effectively. We propose the following contributions to address the challenges in the refinement and continuity of the PWA Lyapunov function.

a) Contributions: The paper introduces two novel methods for dividing cells during the search for valid Lyapunov functions. The first method utilizes the derivative of the Lyapunov function as a criterion to divide a cell, while the second method analyzes the vector field of the PWA dynamics to do so. By examining the behavior of the Lyapunov function derivative or vector field, these methods determine suitable locations for proposing new vertices that will define new cells, since we use the vertex representation for polytopes. Furthermore, the paper proposes using De-

Pouya Samanipour and Hasan A. Poonawala are with the Department of Mechanical and Aerospace Engineering, University of Kentucky, Lexington, USA {samanipour.pouya, hasan.poonawala}@uky.edu. The corresponding author is Hasan A. Poonawala. This work is supported by the Department of Mechanical Engineering at the University of Kentucky.

launay triangulation to automate the refinement process for cells. The proposed refinement methods offer the advantage of finding valid Lyapunov functions with fewer refinements compared to existing techniques. The efficacy of the search procedure is demonstrated through non-trivial examples, where valid Lyapunov functions are successfully identified within reasonable computation times. Additionally, the paper evaluates the effectiveness of the proposed approach in determining the region of attraction (ROA) by comparing the results with other methods. The comparison showcases the capability of the proposed approach to identify the ROA using the PWA Lyapunov functions. The contributions of this paper improve the refinement process addressing challenges in the parameterization of the Lyapunov function.

II. PRELIMINARIES

In this paper, we examine the stability analysis problem for dynamical systems described by piecewise affine functions as follows:

$$\dot{x} = \text{PWA}(x). \quad (1)$$

where $x \in \mathbb{R}^n$ is the state variable, and term PWA denotes a piecewise affine function. We focus on continuous PWA functions with polytopic cells. The rest of this section formally describes PWA functions.

Notation: An index for each element in the set S constitutes the set $I(S)$. The convex hull, the interior, the boundary, and the closure of the set S are denoted by $\text{conv}(S)$, $\text{Int}(S)$, ∂S , and \bar{S} respectively. The transpose of matrix A is A^T . $\langle \cdot, \cdot \rangle$ denotes the inner product, $\angle(\cdot, \cdot)$ is the angle between two vectors, and $\|\cdot\|_2$ is the standard L_2 norm. It should be noted that the symbol \succeq is the element-wise version of \geq .

A. Partitions And Refinements

In this paper, we define a partition \mathcal{P} as a collection of subsets $\{X_i\}_{i \in I(\mathcal{P})}$, where each X_i is a closed subset of \mathbb{R}^n and $\text{int}(X_i) \cap \text{int}(X_j) = \emptyset$, $\forall i, j \in I(\mathcal{P})$ and $i \neq j$. The domain of the partition, $\text{Dom}(\mathcal{P})$, is the union of all the cells in \mathcal{P} .

Given two partitions $\mathcal{P} = \{Y_i\}_{i \in I}$ and $\mathcal{R} = \{Z_j\}_{j \in J}$ of a set $S = \text{Dom}(\mathcal{P}) = \text{Dom}(\mathcal{R})$, we say that \mathcal{R} is a refinement of \mathcal{P} if $Z_j \cap Y_i \neq \emptyset$ implies that $Z_j \subseteq Y_i$. We denote the set of all refinements of \mathcal{P} as $\text{Ref}(\mathcal{P})$ [8].

B. Piecewise Affine Functions

We explicitly parameterize a piecewise affine function $\text{PWA}(x)$ by a partition $\mathcal{P} = \{X_i\}_{i \in I(\mathcal{P})}$ and a collection of matrices $\mathbf{A}_{\mathcal{P}} = \{A_i\}_{i \in I(\mathcal{P})}$ and vectors $\mathbf{a}_{\mathcal{P}} = \{a_i\}_{i \in I(\mathcal{P})}$ such that

$$\begin{aligned} \text{PWA}(x) &= A_i x + a_i, \text{ if } x \in X_i, \text{ where} \\ X_i &= \{x \in \mathbb{R}^n : E_i x + e_i \succeq 0\}. \end{aligned} \quad (2)$$

Note that a generic PWA function may not be continuous unless we appropriately constrain the parameters A_i , a_i , E_i , and e_i [19], [22]. It is assumed that any PWA function in this paper with this explicit form meets such constraints and

Algorithm 1 Verifying Stability using Vertices

Require: PWA(x), Vertices

Solve Optimization Problem (12) with the initial PWA dynamics.

while $\sum_{i=1}^N \tau_i \neq 0$ or Computational time $\leq 3600(\text{sec})$ **do**

for $i \in I_s$ **do**

1- Finding new vertices using presented methods(see IV-D.1).

2- Add the new vertex to B (24).

end for

for $i \in I_{split}$ **do**

1- Finding set of vertices $\mathcal{V}_{new}(i)$ for cell X_i .

2- Forming sub-cells $DT(\mathcal{F}_0(X_i) \cup \mathcal{V}_{new}(i))$ (see (IV-D.2)).

end for

Solve Optimization Problem (12) with the refined PWA dynamics.

end while

return $V(x) = p_i^T x + q_i \quad \forall i \in I(\mathcal{P})$.

is always continuous. Additionally, we consider the origin to be the equilibrium, thus denoting index sets I_0 and I_1 for cells containing and not containing the origin respectively. Also, we assume that all the cells are bounded. Therefore, we can use the vertex representation for all cells. A vertex is a facet of dimension 0 for a cell [23]. Each cell of a partition can be represented using its vertices:

$$X_i = \text{conv}(\mathcal{F}_0(X_i)), \quad (3)$$

where $\mathcal{F}_0(X_i)$ represents the set of vertices of the cell X_i .

III. MAIN ALGORITHM

This section presents an overview of the stability analysis algorithm, which aims to construct an optimization problem to discover the PWA Lyapunov function. The algorithm consists of two main components: the formulation of an optimization problem to find a valid Lyapunov function and a refinement process to enhance the flexibility of the PWA Lyapunov function. A detailed description of these components is provided in the subsequent section. For better comprehension, a pseudo-code representation of the algorithm is presented in **Algorithm 1**. The termination condition of the algorithm is determined by two criteria: either a valid Lyapunov function is found, or the optimization process exceeds the predefined timeout threshold of 3600 seconds. It should be emphasized that in the case of unstable systems, the algorithm needs to be manually terminated.

IV. OPTIMIZATION BASED SEARCH FOR LYAPUNOV FUNCTION

In this section, first, we describe the general idea of the stability analysis and the Lyapunov function. In the next step, we parameterize the Lyapunov function as a PWA function. Then we present the stability condition for PWA dynamics with a PWA candidate Lyapunov function. In IV-C, We

convert the stability analysis problem to a linear optimization problem. We construct the optimization problem to be always feasible; however, only a specific solution is accepted as a valid Lyapunov function. Furthermore, we proposed new refinement approaches **IV-D** to increase the capacity of the candidate Lyapunov functions, facilitating the search for valid Lyapunov functions.

A. Lyapunov function

The Lyapunov stability theory is well known for its application to the analysis of nonlinear dynamical systems [24]. Assume that $V : D \rightarrow R$ is a continuously differentiable function, and $x = 0$ is the equilibrium point of equation (1). In this case, equation (1) will be asymptotically stable if and only if V is strictly positive definite and strictly decreasing $\forall x \in D - \{0\}$.

B. PWA Lyapunov function

In the paper, we investigate the use of PWA Lyapunov functions on a bounded partition that aligns with the PWA dynamics (2) structure. This assumption can be used to further reduce computation costs by taking advantage of the convexity property. Specifically, if all cells in the partition are bounded, an affine function is considered positive on a particular cell X_i if and only if it is positive on all vertices of X_i [19]. This observation allows for simplified analysis and computation of the Lyapunov function. Consider a candidate PWA Lyapunov function such that:

$$V(x) = \begin{cases} p_i^T x + q_i & \text{for } i \in I_1 \\ p_i^T x & \text{for } i \in I_0. \end{cases} \quad (4)$$

In the equation above, the function $V(x)$ is continuous and differentiable in the interior of the cell. It is possible to calculate the derivative of the candidate Lyapunov function, along the dynamic, $\dot{x} = f(x)$, in the interior of cell $X - \{0\}$:

$$\mathcal{L}_f V = \langle \nabla V, f(x) \rangle, \quad (5)$$

where ∇V is the gradient of $V(x)$, and \mathcal{L} is the lie derivative.

When $V(x)$ is differentiable at x , let the local affine Lyapunov function be $V(x) = p^T x + q$, and the dynamics be $\dot{x} = Ax + a$. The derivative of the Lyapunov function along the trajectories can be calculated as follows:

$$\dot{V} = p^T (Ax + a). \quad (6)$$

Lemma 4.1: Let $\{X_i\}_{i \in I}$ be a partition of a bounded subset of \mathbb{R}^n into convex polytopes with vertices v_k .

1) The Lyapunov function (4) will be positive definite iff:

$$\begin{aligned} p_i^T v_k + q_i &> 0 & \text{for } i \in I_1, v_k \in \mathcal{F}_0(X_i) \\ p_i^T v_k &> 0 & \text{for } i \in I_0, v_k \in \mathcal{F}_0(X_i). \end{aligned} \quad (7)$$

2) \dot{V} , (6), will be a negative definite function iff:

$$p_i^T (A_i v_k + a_i) < 0 \text{ for } i \in I(\mathcal{P}), v_k \in \mathcal{F}_0(X_i). \quad (8)$$

Proof: These results can be derived directly as a result of parameterizing the candidate Lyapunov function in the affine form. ■

The last step is to force the Lyapunov function to be continuous. To achieve this goal, the candidate Lyapunov function (4) must meet the following requirements.

$$V_i(v_k) = V_j(v_k), \quad i \neq j \in I(\mathcal{P}), v_k \in \mathcal{F}_0(X_i) \cap \mathcal{F}_0(X_j). \quad (9)$$

Theorem 4.2: A Lyapunov function (4) in the partition \mathcal{P} is considered valid if there exist p_i and q_i satisfy (7)-(9) for every $v_k \neq 0$.

Proof: In this formulation (7) guarantees that the Lyapunov function will be positive definite. Additionally, (9) guarantees continuity. In this case, the Lyapunov function is Lipschitz continuous, but it is not differentiable at the boundary. As a result of the Lipschitz continuity of the Lyapunov function, we are able to use the Clarke generalized gradient and Clarke generalized derivative [25], [26]. According to Clarke generalized gradient $\partial V(x)$ for the PWA Lyapunov function (4) can be described as:

$$\partial V(x) = \text{conv}(\{p_i : i \in I(p), x \in X_i\}) \quad (10)$$

The Clarke generalized derivative along F for the differential inclusion $\dot{x} \in F(x)$ is provided by [25]

$$\dot{V}_F = \{p^T f : p \in \partial V(x), f \in F(x)\}. \quad (11)$$

For points $x \neq 0$ if F is a singleton function then (8) guarantees that $\dot{V}_F < 0$, $\forall p \in \partial V(x)$. As shown by [26], the maximum of the (11) upper-bounded the decrease of the Lyapunov function along solutions of the dynamical systems. Therefore, we may conclude that the Lyapunov function is decreasing along all the trajectories of the PWA dynamical systems. For more detail, please see [8]. ■

The origin is assumed always to be defined as a vertex in I_0 . The assumption that the origin is always defined as a vertex of a cell ensures that we can always find a positive-definite Lyapunov function. Another assumption is that if a vertex $v_k \in \mathcal{F}_0(X_i)$ and $v_k \in X_i \cap X_j$, then $v_k \in \mathcal{F}_0(X_j)$. This assumption is required to preserve the continuity of the Lyapunov function using (9). Details can be found in **IV-D.2**.

C. Optimization problem

The constraints (7)-(9) on variables p_i and q_i from (4) may be infeasible due to conditions (8) associated with the decrease of the Lyapunov function along solutions. Slack variables are added to these constraints to ensure feasibility. Consequently, we can formulate the search process for the PWA Lyapunov function as follows:

$$\min_{p_i, q_i, \tau_i} \sum_{i=1}^N \tau_i \quad (12)$$

Subject to:

$$\begin{aligned} p_i^T (A_i v_k + a_i) - \tau_i &< -\epsilon_1 & \forall i \in I_1, v_k \in \mathcal{F}_0(X_i) \\ p_i^T A_i v_k - \tau_i &< -\epsilon_1 & \forall i \in I_0, v_k \in \mathcal{F}_0(X_i) \\ p_i^T v_k + q_i &> \epsilon_2 & \forall i \in I_1, v_k \in \mathcal{F}_0(X_i) \\ p_i^T v_k &> \epsilon_2 & \forall i \in I_0, v_k \in \mathcal{F}_0(X_i) \\ V_i(v_k) = V_j(v_k) & & \forall v_k \in \mathcal{F}_0(X_i) \cap \mathcal{F}_0(X_j), i \neq j \\ \tau_i &\geq 0 & \forall i \in I(\mathcal{P}) \end{aligned}$$

where τ_i is the slack variable associated to cell X_i , and $\epsilon_1, \epsilon_2 > 0$. By design, we can state the following result.

Lemma 4.3: The optimization problem in (12) is always feasible.

Proof: This result is by the construction of the optimization problem. ■

The solution to this optimization problem yields a valid Lyapunov function if and only if all the slack variables are zero. If the cost function is non-zero, the Lyapunov function is non-decreasing at some vertices. In fact, no Lyapunov function associated with the current partition exists. It may be possible to refine the partition, meaning to divide regions within it, in order to increase the capacity of the Lyapunov function and then repeat the search using this higher-capacity function. In the following section, the refinement process is described in detail.

D. Refinement

A refinement of the current partition is intended to enhance the flexibility of the Lyapunov function search process. To achieve flexibility, a cell X_i with a nonzero slack variable will be divided into smaller sub-cells. In order to keep things simple, we assume that the refinement of X_i will result in the creation of two new subcells, X_{i_1} and X_{i_2} . For each subcell, we can parameterize the PWA Lyapunov function as $V_{i_1} = p_{i_1}^T x + q_{i_1}$ and $V_{i_2} = p_{i_2}^T x + q_{i_2}$. As a result, the candidate Lyapunov function for cell X_i has a higher capacity PWA function that is more flexible. Furthermore, the new PWA Lyapunov function has more parameters, p_i and q_i , as well as constraints. Increasing the number of parameters and constraints might increase the computational complexity for solving (12) since the computational complexity of linear optimization with n parameters and accuracy parameter ϵ is $O(n^{3/4} \log(\frac{n}{\epsilon}))$ [27]. Therefore, to implement refinement, it is necessary to use an intelligent approach, since otherwise, the complexity of the computation may increase.

We utilize a vertex representation for the refinement process to represent cells within a partition, which are convex polytopes. The process of refinement for cells involves adding a new vertex on the cell's boundary and then forming new sub-cells. For this section, we will begin by defining a few concepts and definitions that will be useful for describing these two steps. The first concept is the **simplex region**, a bounded region with the smallest possible number of vertices in \mathbb{R}^d . Polytope's faces of dimension one are called **edges** [23]. In cell X_i , we define the edges by the set $\mathcal{F}_1(X_i)$, and each edge is represented by a pair of vertices (v_j, v_k) , where $v_j, v_k \in \mathcal{F}_0(X_i)$. The edges of convex polytopes can be obtained by using MILP as described in [28]. It is worth emphasizing that the edges containing the origin, where $v_j = 0$ or $v_k = 0$, are not taken into account in the set of edges $\mathcal{F}_1(X_i)$. By making this assumption, we ensure that refinement will not be applied to edges containing the origin. Therefore, if $X_i \in I_0$, its subcells will always contain the origin after refinement.

For the cell X_i , with dynamic $\dot{x} = A_i x + a_i$ and the candidate Lyapunov function $V_i = p_i^T x + q_i$ we can define

the following sets and functions.

- 1) We can find the vector field and the derivative of the Lyapunov function at a vertex, v_j , using the following functions.

$$\dot{x}(X_i, v_j) = A_i v_j + a_i, \quad (13)$$

$$\dot{V}(X_i, v_j) = p_i^T \dot{x}(X_i, v_j), \quad (14)$$

where $\dot{x}(X_i, v_j) \in \mathbb{R}^n$ is the vector field of the local dynamic at the vertex v_j , and $\dot{V}(X_i, v_j)$ is the derivative of the Lyapunov function at the specified vertex in X_i .

- 2) The vertices of the longest edge of a cell can be obtained using the following function:

$$L_{max}(i) = \operatorname{argmax}_{(v_j, v_k) \in \mathcal{F}_1(X_i)} (|v_j - v_k|_2) \quad (15)$$

- 3) The following function can be used to capture changes in the sign of the derivative of a candidate Lyapunov function:

$$sgn_{\dot{V}}(i) = \begin{cases} 1 & \operatorname{sgn}(\dot{V}(X_i, v_j)) \geq 0, \forall v_j \in \mathcal{F}_0(X_i), \\ -1 & \operatorname{sgn}(\dot{V}(X_i, v_j)) \leq 0, \forall v_j \in \mathcal{F}_0(X_i), \\ 0 & \text{otherwise,} \end{cases} \quad (16)$$

where the $\operatorname{sgn}(x)$ is the standard sign function. This function generates zero whenever the sign of the derivative of the candidate Lyapunov function in the cell X_i changes. Otherwise, this function generates either 1 or -1 depending on the sign of the derivative of the candidate Lyapunov function within the cell X_i .

- 4) With $sgn_{\dot{V}}(i)$ being 0, the following set may also be used to provide the vertices of the edges where the sign of the derivative of the Lyapunov function has changed.

$$c_V(i) = \{(v_j, v_k) : sgn_{\dot{V}}(i) = 0, \forall (v_j, v_k) \in \mathcal{F}_1(X_i), \dot{V}(X_i, v_j) \dot{V}(X_i, v_k) < 0\}. \quad (17)$$

There are multiple edges where the sign of the derivative of the Lyapunov function has changed if $sgn_{\dot{V}}(i) = 0$.

- 5) The following equation can be used to determine the vertices for an edge with the largest variation in the derivative of a candidate Lyapunov function.

$$\Delta \dot{V}_{max}(i) = \{(v_j, v_k) : \operatorname{argmax}_{(v_j, v_k) \in \mathcal{F}_1(X_i)} |\dot{V}(X_i, v_j) - \dot{V}(X_i, v_k)|\}. \quad (18)$$

- 6) We aim to determine the edge along which the vector fields exhibit the greatest range of angle variations. Therefore, we use the following function to find the edge with the smallest cosine between the vector field at its vertices.

$$cos_{min}(i) = \{(v_j, v_k) : \operatorname{argmin}_{(v_j, v_k) \in \mathcal{F}_1(X_i)} \frac{\langle \dot{x}(X_i, v_j), \dot{x}(X_i, v_k) \rangle}{|\dot{x}(X_i, v_j)|_2 |\dot{x}(X_i, v_k)|_2}\} \quad (19)$$

Now, we can delve into the refinement process.

Algorithm 2 Finding new vertices using naive refinement

Require: PWA(x), Vertices

1- Find

$$i = \operatorname{argmax}_{i \in I_s}(\tau_i) \quad (21)$$

2- Find (v_j, v_k) using $L_{max}(i)$ (15).3- finding v_{new_i} using (20) where $\alpha = \beta = 0.5$.**return** v_{new_i}, \dot{i} .

1) *Finding new vertices:* The first step in the refinement process is to introduce new vertices on the boundary of cells in $I_s = \{i \in I: \tau_i > 0\}$. The new vertex for the cell X_i can be obtained using the following equation:

$$v_{new_i} = \alpha v_j + \beta v_k, \quad (20)$$

which is a linear combination of two vertices of an edge. Based on the splitting approach which will be introduced in this section, α, β, v_j , and v_k in (20) could be different. Here we consider three different approaches for finding the new vertices.

a) *Naive refinement:* The first algorithm is inspired from [19]. The original algorithm was described for simplex regions and restricted to 2-D problems. In order to make the comparison possible we generalize the method for all types of regions. The process of refinement for the cell X_i based on [19] is described in **Algorithm 2**. The naive algorithm adds a new vertex exclusively to the longest edge, denoted as L_{max} , of cell X_i that has the largest slack variable, as determined by (21). This method creates sub-cells with the largest possible volume without considering the candidate Lyapunov function or local dynamics. Consequently, it may lead to unsatisfactory results. Selecting vertices randomly could increase computational complexity without necessarily improving the refinement process. Thus, it is crucial to choose new vertices intelligently.

b) *Lyapunov-based refinement:* To address the challenge with the naive refinement, a new approach is proposed, leveraging the candidate Lyapunov function to make more informed decisions regarding selecting new vertices. The basic principle behind this method is that for every cell X_i where $i \in I_s$ finding a set of points $P(i) = \{v_{new_i} : \dot{V}(X_i, v_{new_i}) = 0, v_{new_i} \in \partial X_i\}$. Using these points, $v_{new_i} \in P(i)$, the cell X_i could be divided into the two sub-cells, X_{i_1} and X_{i_2} , where $sgn_{\dot{V}}(i_2) = -sgn_{\dot{V}}(i_1)$. In the case of $sgn_{\dot{V}}(i) = 0$, we know that $P(i) \neq \emptyset$. Therefore, we can find these points using the following convex problem in cell X_i .

$$\begin{aligned} & \max_{\alpha, \beta} \quad 0 & (22) \\ & \text{s.t.} \quad \alpha \dot{V}(X_i, v_j) + \beta \dot{V}(X_i, v_k) = 0, \\ & \quad \alpha + \beta = 1, \\ & \quad 0 \leq \alpha, \beta \leq 1, \\ & \quad (v_j, v_k) \in \mathcal{F}_1(X_i). \end{aligned}$$

Algorithm 3 Finding new vertices using Lyapunov-based refinement

Require: PWA(x), Vertices**for** $i \in I_s$ **do**1- Finding $sgn_{\dot{V}}(i)$ using (16).**if** $sgn_{\dot{V}}(i) = 0$ **then****for** $(v_j, v_k) \in c_V(i)$ **do**1- Solve the convex problem (22) to obtain α and β .2- Find v_{new_i} using (20).**end for****else**1- Find (v_j, v_k) using $\Delta \dot{V}_{max}(i)$ (18).2- Find v_{new_i} using (20) where $\alpha = \beta = 0.5$.**end if****end for****return** v_{new_i}, \dot{i} .

An explanation of how to find i, v_j and v_k in (22) and other details about finding a new vertex using Lyapunov-based refinement can be found in **Algorithm 3**. If $sgn_{\dot{V}}(i) = 1$, then $P(i) = \emptyset$, so we choose the new vertex at the edge obtained from $\Delta \dot{V}_{max}(i)$.

In contrast to the previous method that focused only on the cell with the largest slack variable, the Lyapunov-based refinement is now applied to all cells with nonzero slack variables, denoted as $i \in I_s$. As a result of this broader approach, each relevant cell will be refined based on its individual candidate Lyapunov function. However, it is important to note that the coefficient vector p_i used in the refinement process may change significantly in the next iteration. Therefore, this approach may not be suitable in all cases, as the optimization process in the subsequent steps can alter the candidate Lyapunov function.

c) *Vector field refinement:* To address the problem with the Lyapunov-based refinement, the search for new vertices should be conducted using a method that is not influenced by the optimization process in the subsequent steps. The proposed method leverages the vector field information of the dynamics, which remains unchanged during the optimization process. The underlying heuristic behind this method is that the direction or magnitude of the vector fields along an edge may undergo significant changes within a cell X_i where $i \in I_s$. Consequently, a higher-capacity PWA function may be required to represent the Lyapunov function within X_i accurately. As illustrated in Fig.1, the vector field direction in a cell can exhibit substantial variations, such as a flip from v_1 to v_2 . In such cases, a simple PWA function may struggle to approximate the level set accurately. To mitigate this, the method is adding a new vertex, v_{new_i} , between (v_1, v_2) where $\angle(\dot{x}(X_i, v_1), \dot{x}(X_i, v_{new_i})) = \angle(\dot{x}(X_i, v_2), \dot{x}(X_i, v_{new_i}))$. Consequently, after each refinement process, the greatest angle between the vector fields of an edge in cell X_i is divided in half. The process of finding a new vertex using the vector field refinement is outlined in

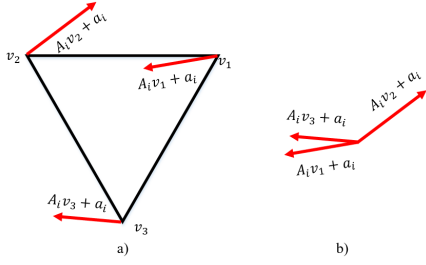


Fig. 1. Vector fields of a cell on its vertices. b) The angle between vector fields of vertices. As can be seen, the angle of the vector field between v_1 and v_2 is close to $-\pi$.

Algorithm 4 Finding new vertices using Vector field refinement

Require: $PWA(x)$, Vertices

for $i \in I_s$ **do**

1- Find (v_j, v_k) using (19).

2- Find α and β using following equation:

$$\alpha = \frac{1}{1 + \frac{|\dot{x}(X_i, v_j)|_2}{|\dot{x}(X_i, v_k)|_2}}, \beta = 1 - \alpha. \quad (23)$$

3- Find the new vertex using (20)

end for

return v_{new_i}, i .

Algorithm 4, which provides a detailed description of the method.

Before moving on to the next step, storing the new vertices created by these algorithms in the following buffer is necessary.

$$B = \{v_{new_i} \in \mathbb{R}^n : i \in I_s\}. \quad (24)$$

Now we can proceed to the next step, which is forming sub-cells.

2) *Forming sub-cells:* In order to form sub-cells, Johannson [19] proposed remedies for 2-D systems; however, this method is limited to simplex cells. It was suggested that triangulation methods be used for non-simplex regions in [19], but no specific method or implementation is presented. It has also been proposed in [29] to apply Delaunay triangulation to all cells; however, the results have been limited to 2-D examples. We apply Delaunay triangulation to overcome the challenges associated with forming sub-cells for non-simplex cells and cells in higher dimensions ($n > 2$), which would be challenging to accomplish manually.

The Delaunay triangulation of a set of points in \mathbb{R}^d is defined to be the triangulation such that the circumcircle of every triangle in the triangulation contains no point from the set in its interior. Such a unique triangulation exists for every point set in \mathbb{R}^d , and it is the dual of the Voronoi diagram. Moreover, the Delaunay triangulation will maximize the minimum angle in each triangle [30]. $DT(\mathcal{F}_0(X_i))$ is the notation for implementing Delaunay triangulation using

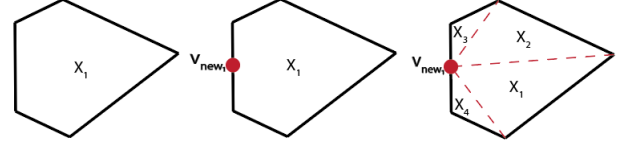


Fig. 2. Triangulation process using Delaunay. a) A non-simplex region b) Midpoint is chosen to be added as a new vertex. c) The refined cells generated by the Delaunay triangulation.

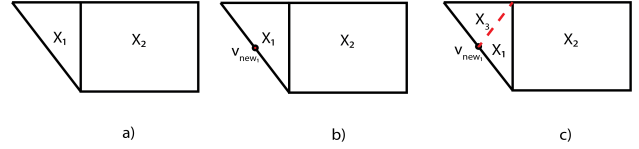


Fig. 3. The process of refinement using naive refinement a) Two adjacent cells where $\tau_1 > \tau_2 > 0$. b) Based on the naive refinement method, the new vertex is located on the longest edge of the cell X_1 because it has the greatest slack variable τ_1 . c) Delaunay triangulation is used to form the sub-cells.

the vertices of the cell X_i . The process of implementing Delaunay triangulation for a single cell is illustrated in Fig. 2. Delaunay triangulation will also handle the continuity of the Lyapunov function if the partition is composed of multiple cells. To illustrate how continuity is preserved, let us consider the v_{new_i} as the new vertex obtained using (20) for the cell X_i . If $v_{new_i} \in X_i \cap X_j$, then v_{new_i} must also be considered as a new vertex for the cell X_j , and $DT(\mathcal{F}_0(X_i) \cup v_{new_i})$ and $DT(\mathcal{F}_0(X_j) \cup v_{new_i})$ should be implemented. Consequently, even after refinement, continuity would be guaranteed by (9). Generally, in order to implement Delaunay triangulation within the current partition, we have to follow the following steps.

1) First, we must obtain the following set containing cells that required refinement.

$$I_{split} = \{i : X_i \cap B \neq \emptyset, i \in I(\mathcal{P})\}. \quad (25)$$

2) Then, we need to find the vertices located on the boundary of the cell X_i where $i \in I_{split}$ using the following set.

$$\mathcal{V}_{new}(i) = \{v_{new_j} : v_{new_j} = X_i \cap B, i \in I_{split}\}. \quad (26)$$

3) Then, we can form the new sub-cells using $DT(\mathcal{F}_0(X_i) \cup \mathcal{V}_{new}(i))$ for $i \in I_{split}$.

The process of refinement based on the naive approach using Delaunay triangulation is shown in Fig. 3. As can be seen, the sub-cells are created just in the simplex cells. However, the Lyapunov-based and vector-field methods perform differently as shown in Fig. 4. and Fig. 5. respectively.

V. RESULTS

The paper presents seven examples to demonstrate the search performance for a PWA Lyapunov function using the algorithm described in **Algorithm 1**. The computations

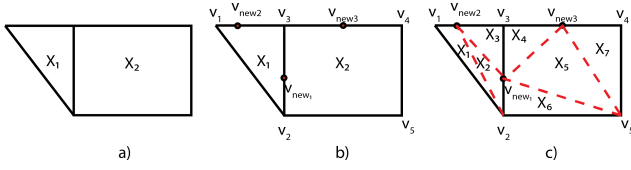


Fig. 4. The process of refinement using Lyapunov-based refinement a) Two adjacent cells where $\tau_1 > \tau_2 > 0$. b) Let's assume in the simplex cell, X_1 , we have $\dot{V}(X_1, v_2) < 0 < \dot{V}(X_1, v_1) < \dot{V}(X_1, v_3)$ and in the non-simplex-cell, X_2 , $0 < \dot{V}(X_2, v_3) < \dot{V}(X_2, v_2) < \dot{V}(X_2, v_5) < \dot{V}(X_2, v_4)$. Based on the Lyapunov-based refinement method, the new vertices, V_{new1} and V_{new2} , for the simplex cell will be obtained using (22) on the edges obtained using (17). For the non-simplex cell, the new vertex V_{new3} is obtained using (20) where $\alpha = \beta = 0.5$ on the edge obtained using (18) c) Delaunay triangulation is used to form the sub-cells for the cell X_1 and X_2 with their new vertices. Delaunay Triangulation for the cell X_1 and X_2 will be $DT(\mathcal{F}_0(X_1) \cup v_{new1} \cup v_{new2})$ and $DT(\mathcal{F}_0(X_2) \cup v_{new1} \cup v_{new3})$ respectively.

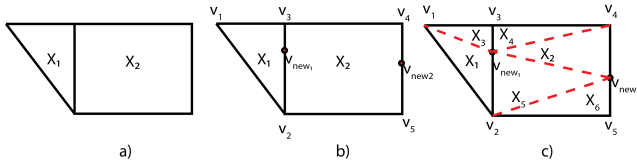


Fig. 5. The process of refinement using vector field refinement a) Two adjacent cells where $\tau_1 > \tau_2 > 0$. b) Let's assume in the simplex cell we have the biggest variation in the vector field angle, $\cos_{min}(1) = (v_2, v_3)$, and in the non-simplex cell the biggest variation of the vector field, $\cos_{min}(2) = (v_4, v_5)$. Based on the vector field refinement method, the new vertex for the simplex and non-simplex cell will be obtained using (20) with α and β obtained from (23). c) The Delaunay triangulation is employed to form the sub-cells for the cell X_1 and X_2 using $DT(\mathcal{F}_0(1) \cup v_{new1})$ and $DT(\mathcal{F}_0(2) \cup v_{new1} \cup v_{new2})$ respectively.

are implemented using the Mosek optimization package [31] and Python 3.9 on a computer with a 2.1 GHz processor and 8 GB RAM. During the computations, a tolerance of 10^{-8} is used to determine if a number is nonzero. In all the examples, the values of ϵ_1 and ϵ_2 are set to 10^{-4} . These examples aim to showcase the effectiveness and efficiency of the proposed algorithm in finding valid Lyapunov functions within reasonable computation times.

Example 1 (4-D Example [13]): For this example, we will use the 4-D MPC example presented in [13] as follows:

$$x_{t+1} = \begin{bmatrix} 0.4346 & -0.2313 & -0.6404 & 0.3405 \\ -0.6731 & 0.1045 & -0.0613 & 0.3400 \\ -0.0568 & 0.7065 & -0.086 & 0.0159 \\ 0.3511 & 0.1404 & 0.2980 & 1.0416 \end{bmatrix} x_t + [0.4346, -0.6731, -0.0568, 0.3511] u_t. \quad (27)$$

It includes the same details as [13], such as a state constraint of $\|x\|_\infty \leq 4$, an input constraint of $\|u\|_\infty \leq 1$, a prediction horizon of $T = 10$, a stage cost of $Q = 10I$ and $R = 1$. Explicit MPC produces a PWA dynamic with 193 cells. To ensure that the origin is a vertex, we refined the cell with the origin on its interior first. Our next step is to convert the discrete-time PWA dynamics into continuous-time PWA dynamics with a sampling time $t_s = 0.01$. Finally, We

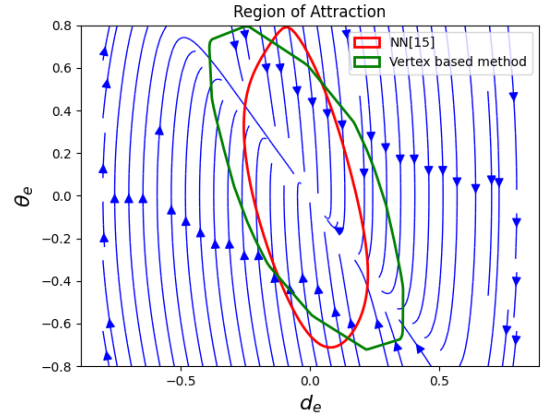


Fig. 6. The ROA for the closed-loop path following wheeled vehicle using NN [15] and vertex-based method.

searched for the continuous PWA Lyapunov function using **Algorithm 1** with all refinement techniques. The **Algorithm 1** timed out after 2000 seconds using the naive refinement after 31 iterations. **Algorithm 1** found the Lyapunov function in 1200 seconds using the Lyapunov-based refinement with 5874. With the vector field refinement, the **Algorithm 1** found the solution in 280 seconds by generating 3086 cells. In comparison with [13], the Lyapunov function using vector-field refinement requires a shorter computational time.

Example 2 (4-D controllable canonical dynamic):

Following is a simple 4-D example with stable canonical controllable dynamics with condition number 10 to illustrate the meaningful difference between the refinement methods.

$$\dot{x} = \begin{bmatrix} 0 & 1 & 0 & 0 \\ 0 & 0 & 1 & 0 \\ 0 & 0 & 0 & 0 \\ -24 & -50 & -35 & -10 \end{bmatrix} x, \quad (28)$$

where $\|x\|_\infty \leq 5$ and the initial partition includes 16 simplex cells around the origin with the dynamic (28). The search **Algorithm 1** found the valid PWA Lyapunov function after 43 seconds with 1054 cells created as a result of vector field refinement, whereas Lyapunov-based refinement required 106 seconds with 2743 cells, and naive search required 1546 seconds with 6943 cells.

Example 3 (Path Following Wheeled Vehicle [15]):

The following kinematic model is used to analyze the stability of a path following wheeled vehicle in [15]:

$$\begin{aligned} \dot{d}_e &= \nu \sin(\theta_e), \\ \dot{\theta}_e &= \omega - \frac{\nu \kappa(s) \cos(\theta_e)}{1 - d_e \kappa(s)}. \end{aligned} \quad (29)$$

In equation (29), we have the state variables θ_e , which represents the angle error, and d_e , which represents the distance error. The control input is denoted as ω . In this study, we used a single-hidden layer ReLU with 50 neurons as described in [8] in order to identify the dynamic (29) with the NN controller [15] in the region $\|x\|_\infty \leq 0.8$. Moreover, we used the vertex-based method along with vector field

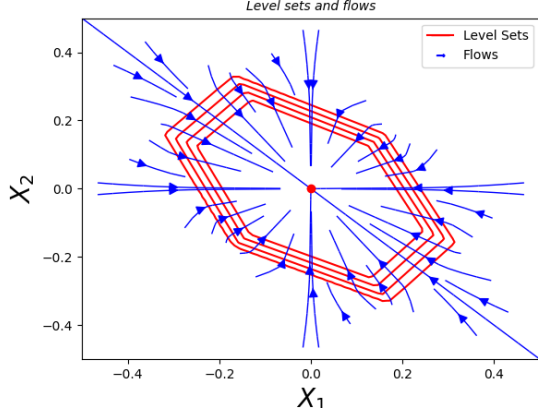


Fig. 7. Selected level sets and flows for the Example 4.

refinement to obtain the PWA Lyapunov function. As can be seen in Fig. 6, a comparison was made between the ROA obtained by the proposed method and the ROA obtained using the NN Lyapunov function [15].

Example 4 (Multi-agent consensus): The Hegselmann-Krause model is a widely studied model in the literature, which involves N autonomous agents with state variables ξ_i . Each agent's dynamics are given by the equation:

$$\dot{\xi}_i = \sum_{j=1}^N \phi(\xi_i, \xi_j)(\xi_j - \xi_i) \quad (30)$$

where i ranges from 1 to N , and $\phi : [0, 1]^2 \rightarrow \{0, 1\}$ represents a weight function as defined in the reference [17]. The stability analysis results for this model are presented in Fig. 7. We observed that a valid PWA Lyapunov function can be obtained without requiring any refinement. Therefore, the choice of different splitting approaches does not have any impact on this particular example. The details are provided in Table I.

Example 5 (2-D example from [25], [21], [19]): This system has been presented in four different regions as follows:

$$\begin{aligned} Z_1 &= \{x \in \mathbb{R}^2 : -x_1 + x_2 \geq 0, x_1 + x_2 \geq 0\} \\ Z_2 &= \{x \in \mathbb{R}^2 : -x_1 + x_2 \geq 0, -x_1 - x_2 \geq 0\} \\ Z_3 &= \{x \in \mathbb{R}^2 : x_1 - x_2 \geq 0, -x_1 - x_2 \geq 0\} \\ Z_4 &= \{x \in \mathbb{R}^2 : x_1 - x_2 \geq 0, x_1 + x_2 \geq 0\} \end{aligned} \quad (31)$$

and the dynamics are as follows:

$$\Omega_p : \dot{x} = \begin{cases} \begin{bmatrix} -0.1 & 1 \\ -5 & -0.1 \end{bmatrix} x & \text{if } x \in Z_1 \text{ or } x \in Z_3 \\ \begin{bmatrix} -0.1 & 5 \\ -1 & -0.1 \end{bmatrix} x & \text{if } x \in Z_2 \text{ or } x \in Z_4. \end{cases} \quad (32)$$

The level sets and the vector fields are shown in Fig. 8. The PWA Lyapunov function was obtained by refining the cells. In this example, all three refinement methods perform similarly in finding the Lyapunov function. The details about

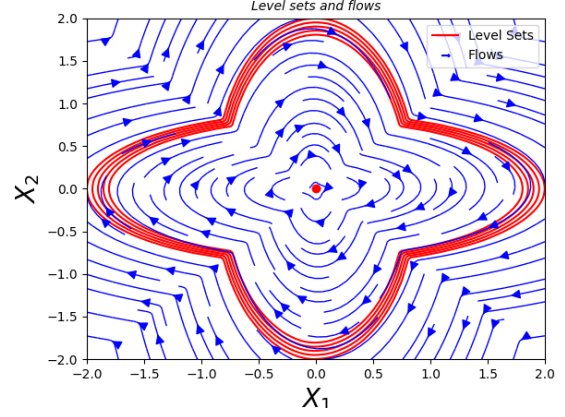


Fig. 8. Selected level sets and flows of the Example 5.

this example are presented in Table I. The refinement process creates 128 cells in the partition.

Example 6 (Explicit model-predictive controller [8]):

In this study, the stability of the following discrete time dynamic is investigated using explicit MPC, similar to [8], [13].

$$x_{t+1} = \begin{bmatrix} 1 & 1 \\ 0 & 1 \end{bmatrix} x_t + \begin{bmatrix} 1 \\ 0.5 \end{bmatrix} u_t \quad (33)$$

As in [8], the MPC problem has the same specification such as stage cost, actuator, and state constraints. We use the MPT3 toolbox [32] in Matlab to obtain an explicit controller. A sampling time of $t_s = 0.01s$ was used to obtain the continuous form of the dynamic (33) with the explicit MPC controller. The PWA dynamics generated by the explicit MPC have a cell where the origin is not on the vertices. As a result, we refine this cell with the origin as a new vertex, $DT(\mathcal{F}_0(X_i) \cup 0)$, and then start the **Algorithm 1**. Fig. 9 depicts the level sets of the Lyapunov function. The Lyapunov function was found by all three refinement algorithms within one second. The Lyapunov-based refinement and the vector-field refinement, however, produce a greater number of cells than the naive refinement.

Example 7 (Inverted Pendulum [8], [33], [34]): It is common in the literature to use an inverted pendulum as an example with the following state-space model:

$$\begin{bmatrix} \dot{x}_1 \\ \dot{x}_2 \end{bmatrix} = \begin{bmatrix} x_2 \\ -\frac{c}{m}x_2 - gl^2 \sin(x_1) \end{bmatrix} + \begin{bmatrix} 0 \\ \frac{1}{ml^2} \end{bmatrix} u \quad (34)$$

where $m = 0.15$ kg, $l = 0.5$ m, $c = 0.1Ns/rad$, and $g = 9.81$ m/s² [15]. First, we used a single-hidden layer ReLU neural network consisting of 20 neurons in the region $\|x\|_\infty \leq 4$ to identify the uncontrolled dynamics. Subsequently, we designed a ReLU neural network controller as described in [8]. By incorporating the ReLU NN controller into the system, we were able to achieve stability. We searched for the PWA Lyapunov function using **Algorithm 1** with the Vector-field refinement. The results are compared with Linear-quadratic regulator (LQR) [34] and NN

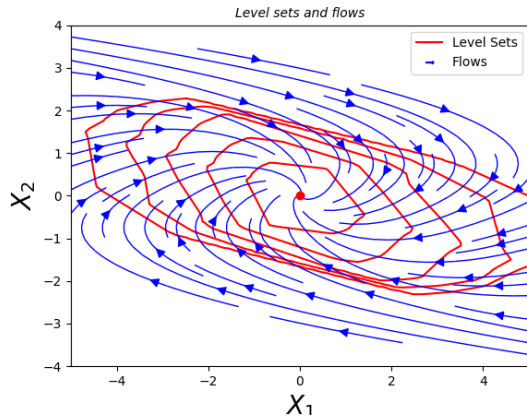


Fig. 9. Selected level sets and flows for the Example 6.

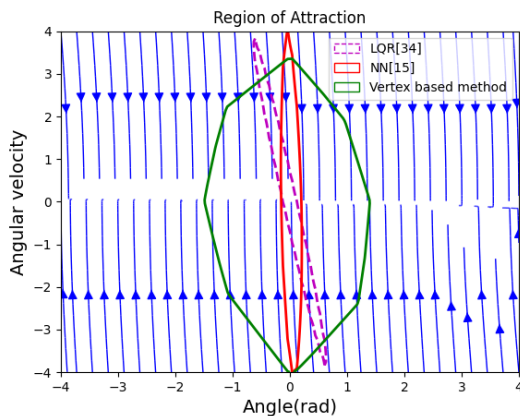


Fig. 10. The ROA for the closed-loop inverted pendulum using LQR [34], NN [15] and vertex-based method.

Lyapunov function [15] in Fig.10. The Lyapunov function obtained using the proposed approach has a larger ROA. It is important to note that the valid region for [34] and [15] is $\|x\|_2 \leq 4$.

Moreover, the computational time for each example is presented in the TABLE I. Having run each simulation ten times, the computational time is the average time elapsed. TABLE I provides the number of cells created by each refinement technique. The Vector field refinement performs better in terms of computation time and number of cells than the Lyapunov-based and naive approaches specifically in 4-D examples.

VI. DISCUSSION

We have shown the effectiveness of our automated approach for stability verification through various examples. Our proposed refinement methods outperform existing techniques, and although our method does not specifically aim to maximize the region of attraction, our results are comparable to other methods. However, there are challenges to consider when applying this algorithm to a wider range of problems.

Examples	Naive approach		Lyapunov based		Vector field	
	Time	cells	Time	Cells	Time	Cells
Example 1	Timed-out	17764	1200	5874	280	3086
Example 2	1546	6943	106	2743	43	1054
Example 3	17.6	705	14.5	649	11.2	532
Example 4	0.15	12	0.15	12	0.15	12
Example 5	1.8	116	1.8	116	1.86	120
Example 6	1.27	88	1.27	88	1.29	96
Example 7	23.3	1107	17.4	996	16.1	956

TABLE I

SUMMARY OF EXAMPLES OF APPLYING THE PROPOSED METHODS. ALL TIMES ARE IN SECONDS.

Limitations: The computational complexity and performance of the proposed algorithm depend on the increase in the number of cells and optimization parameters during the refinement process. In a space \mathbb{R}^n , the number of cells should satisfy $m \geq 2^n$. The simplest case, where the origin is surrounded by 2^n simplex cells, results in an optimization problem with $2^n \times (n+1)$ parameters and $2^{n+1} \times n$ inequality constraints. The number of constraints increases with the presence of non-simplex cells. The computational complexity of the optimization process significantly depends on the dimensionality n , leading to longer computation times as cells are further divided. In some cases, the algorithm may encounter challenges and longer computation times due to increased complexity. To compare the results of different examples in terms of computational time and the number of cells, we introduce the following concepts:

$$T_{opt_i} = \frac{\sum_{j=1}^i t_{optj}}{\sum_{i=1}^N t_{opt_i}} \quad (35)$$

$$Nr_i = \frac{n_{r_i}}{\sum_{i=1}^N n_{r_i}}. \quad (36)$$

T_{opt} represents the normalized accumulative optimization time, N_r indicates the normalized number of regions, t_{opt} represents the time spent finding the solution with MOSEK, n_r represents the number of regions, and N represents the total number of iterations to solve the optimization problem. The subscripts i and j indicate the optimization iteration. The relationship between the normalized accumulative optimization time (T_{opt}) and the normalized number of cells (N_r) is investigated in three different examples in Fig.11. The graphs demonstrate almost linear behavior for Example 6 and Example 5, while Example 1 exhibits an almost exponential trend. This indicates that increasing the number of cells could present a significant challenge for our proposed technique. Additionally, the refinement process may result in cells with nearly coplanar vertices, which can introduce numerical difficulties. It is essential to consider these complexities and challenges when applying our algorithm to various systems.

VII. CONCLUSION

This paper presents a computational framework for obtaining valid PWA Lyapunov functions. The framework

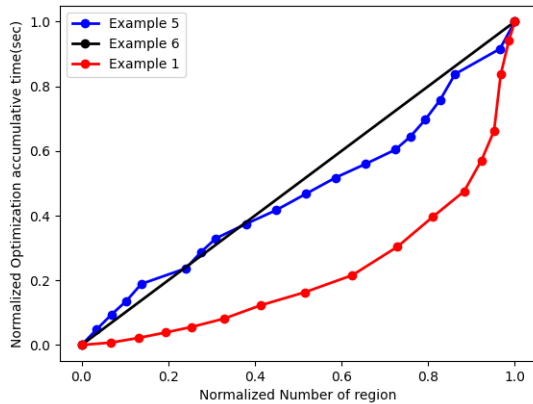


Fig. 11. normalized Accumulative time for optimization vs. the normalized number of regions. The accumulative optimization time with respect to the number of cells for 2-D examples is almost linear; however, in the 4-D example, the accumulative time grows exponentially with respect to the number of cells.

addresses the challenges of formulating the Lyapunov conditions as a linear optimization problem, which does not always guarantee a valid Lyapunov function. To overcome this limitation, two novel refinement methods are proposed, enhancing the flexibility of the candidate Lyapunov function. We used the Delaunay triangulation to automate the refinement process. We demonstrated that the proposed approach is effective based on experiments and comparisons with alternative approaches. The experiments successfully solve a 4-D example in a short time, highlighting the practicality and efficiency of the framework. The proposed framework offers a more effective method for generating valid PWA Lyapunov functions, offering flexibility through refinement methods and automating the process.

REFERENCES

- [1] T. Marcucci, R. Deits, M. Gabiccini, A. Bicchi, and R. Tedrake, "Approximate hybrid model predictive control for multi-contact push recovery in complex environments," in *2017 IEEE-RAS 17th International Conference on Humanoid Robotics (Humanoids)*. IEEE, 2017, pp. 31–38.
- [2] X. Sun, H. Zhang, Y. Cai, S. Wang, and L. Chen, "Hybrid modeling and predictive control of intelligent vehicle longitudinal velocity considering nonlinear tire dynamics," *Nonlinear Dynamics*, vol. 97, no. 2, pp. 1051–1066, 2019.
- [3] A. Bemporad, F. Borrelli, and M. Morari, "Piecewise linear optimal controllers for hybrid systems," in *Proceedings of the 2000 American Control Conference. ACC (IEEE Cat. No. 00CH36334)*, vol. 2. IEEE, 2000, pp. 1190–1194.
- [4] J. Qiu, W. Ji, H.-K. Lam, and M. Wang, "Fuzzy-affine-model-based sampled-data filtering design for stochastic nonlinear systems," *IEEE transactions on fuzzy systems*, vol. 29, no. 11, pp. 3360–3373, 2020.
- [5] A. Alessio and A. Bemporad, "A survey on explicit model predictive control," *Nonlinear Model Predictive Control: Towards New Challenging Applications*, pp. 345–369, 2009.
- [6] Í. Elguea-Aguinaco, A. Serrano-Muñoz, D. Chrysostomou, I. Inziarte-Hidalgo, S. Bøgh, and N. Arana-Arexolaleiba, "A review on reinforcement learning for contact-rich robotic manipulation tasks," *Robotics and Computer-Integrated Manufacturing*, vol. 81, p. 102517, 2023.
- [7] I. Jebellat, H. N. Pishkenari, and E. Jebellat, "Training microrobots via reinforcement learning and a novel coding method," in *2021 9th RSI International Conference on Robotics and Mechatronics (ICRoM)*. IEEE, 2021, pp. 105–111.

- [8] P. Samanipour and H. A. Poonawala, "Stability analysis and controller synthesis using single-hidden-layer relu neural networks," *IEEE Transactions on Automatic Control*, 2023.
- [9] A. Abate, D. Ahmed, M. Giacobbe, and A. Peruffo, "Formal synthesis of lyapunov neural networks," *IEEE Control Systems Letters*, vol. 5, no. 3, pp. 773–778, 2020.
- [10] M. Korda, "Stability and performance verification of dynamical systems controlled by neural networks: algorithms and complexity," *IEEE Control Systems Letters*, 2022.
- [11] H. Ravanbakhsh and S. Sankaranarayanan, "Learning lyapunov (potential) functions from counterexamples and demonstrations," *arXiv preprint arXiv:1705.09619*, 2017.
- [12] M. Fazlyab, M. Morari, and G. J. Pappas, "Safety verification and robustness analysis of neural networks via quadratic constraints and semidefinite programming," *IEEE Transactions on Automatic Control*, 2020.
- [13] S. Chen, M. Fazlyab, M. Morari, G. J. Pappas, and V. M. Preciado, "Learning lyapunov functions for hybrid systems," in *Proceedings of the 24th International Conference on Hybrid Systems: Computation and Control*, 2021, pp. 1–11.
- [14] H. Dai, B. Landry, L. Yang, M. Pavone, and R. Tedrake, "Lyapunov-stable neural-network control," *arXiv preprint arXiv:2109.14152*, 2021.
- [15] R. Zhou, T. Quartz, H. De Sterck, and J. Liu, "Neural lyapunov control of unknown nonlinear systems with stability guarantees," *arXiv preprint arXiv:2206.01913*, 2022.
- [16] J. Anderson and A. Papachristodoulou, "Advances in computational lyapunov analysis using sum-of-squares programming," *Discrete & Continuous Dynamical Systems-B*, vol. 20, no. 8, p. 2361, 2015.
- [17] R. Iervolino, D. Tangredi, and F. Vasca, "Lyapunov stability for piecewise affine systems via cone-copositivity," *Automatica*, vol. 81, pp. 22–29, 2017.
- [18] R. Iervolino, S. Trenn, and F. Vasca, "Asymptotic stability of piecewise affine systems with filippov solutions via discontinuous piecewise lyapunov functions," *IEEE Transactions on Automatic Control*, vol. 66, no. 4, pp. 1513–1528, 2020.
- [19] M. Johansson, "Piecewise linear control systems," Ph.D. dissertation, Ph. D. Thesis, Lund Institute of Technology, Sweden, 1999.
- [20] H. A. Poonawala, "Stability analysis via refinement of piecewise linear lyapunov functions," in *2019 IEEE 58th Conference on Decision and Control (CDC)*, 2019, pp. 1442–1447.
- [21] —, "Stability analysis of conewise affine dynamical systems using conewise linear lyapunov functions," in *2021 American Control Conference (ACC)*. IEEE, 2021, pp. 2406–2411.
- [22] H. A. Poonawala, N. Lauffer, and U. Topcu, "Training classifiers for feedback control with safety in mind," *Automatica*, vol. 128, p. 109509, 2021.
- [23] M. Henk, J. Richter-Gebert, and G. M. Ziegler, "Basic properties of convex polytopes," in *Handbook of discrete and computational geometry*. Chapman and Hall/CRC, 2017, pp. 383–413.
- [24] H. K. Khalil, *Nonlinear control*. Pearson New York, 2015, vol. 406.
- [25] M. Della Rossa, A. Tanwani, and L. Zaccarian, "Smooth approximation of patchy lyapunov functions for switched systems," *IFAC-PapersOnLine*, vol. 52, no. 16, pp. 364–369, 2019.
- [26] R. Baier, L. Grüne, and S. Freyr Hafstein, "Linear programming based lyapunov function computation for differential inclusions," 2012.
- [27] M. El Ghami, Z. Guennoun, S. Bouali, and T. Steihaug, "Interior-point methods for linear optimization based on a kernel function with a trigonometric barrier term," *Journal of Computational and Applied Mathematics*, vol. 236, no. 15, pp. 3613–3623, 2012.
- [28] J. Zago, E. Camponogara, and E. Antonelo, "Vertex-based reachability analysis for verifying relu deep neural networks," *arXiv preprint arXiv:2301.12001*, 2023.
- [29] M. Rubagotti, S. Trimboli, D. Bernardini, and A. Bemporad, "Stability and invariance analysis of approximate explicit mpc based on pwa lyapunov functions," *IFAC Proceedings Volumes*, vol. 44, no. 1, pp. 5712–5717, 2011.
- [30] V. T. Rajan, "Optimality of the delaunay triangulation in rd," in *Proceedings of the seventh annual symposium on Computational geometry*, 1991, pp. 357–363.
- [31] M. ApS, "Mosek optimizer api for python," *Version*, vol. 9, no. 17, pp. 6–4, 2022.
- [32] M. Kvasnica, P. Grieder, M. Baotić, and M. Morari, "Multi-parametric toolbox (mpt)," in *Hybrid Systems: Computation and Control: 7th*

International Workshop, HSCC 2004, Philadelphia, PA, USA, March 25-27, 2004. Proceedings 7. Springer, 2004, pp. 448–462.

- [33] M. Farsi, Y. Li, Y. Yuan, and J. Liu, “A piecewise learning framework for control of unknown nonlinear systems with stability guarantees,” in *Learning for Dynamics and Control Conference*. PMLR, 2022, pp. 830–843.
- [34] Y.-C. Chang, N. Roohi, and S. Gao, “Neural lyapunov control,” *Advances in neural information processing systems*, vol. 32, 2019.